

Near-IR Search for Lensed Supernovae Behind Galaxy Clusters

II. First Detection and Future Prospects

A. Goobar¹, K. Paech¹, V. Stanishev^{1,2}, R. Amanullah¹, T. Dahlén³, J. Jönsson^{1,4}, J. P. Kneib⁵, C. Lidman⁶,
M. Limousin⁷, E. Mörtzell¹, S. Nobili¹, J. Richard⁸, T. Riehm⁹, and M. von Strauss^{1,*}

¹ Department of Physics, Stockholm University, Albanova University Center, S-106 91 Stockholm, Sweden

² CENTRA - Centro Multidisciplinar de Astrofísica, Instituto Superior Técnico, Av. Rovisco Pais 1, 1049-001 Lisbon, Portugal

³ Space Telescope Science Institute, Baltimore, MD 21218, USA

⁴ University of Oxford Astrophysics, Denys Wilkinson Building, Keble Road, Oxford OX1 3RH, UK

⁵ Laboratoire d'Astrophysique de Marseille, OAMP, CNRS-Université Aix-Marseille, 38, rue Frédéric Joliot-Curie, 13388 Marseille cedex 13, France

⁶ ESO, Vitacura, Alonso de Cordova, 3107, Casilla 19001, Santiago, Chile

⁷ Dark Cosmology Centre, Niels Bohr Institute, University of Copenhagen, Juliane Maries Vej 30, DK-2100 Copenhagen, Denmark

⁸ Department of Astronomy, California Institute of Technology, 105-24, Pasadena, CA 91125, USA

⁹ Stockholm Observatory, Stockholm University, Albanova University Center, S-106 91 Stockholm, Sweden

Received January 26, 2023; accepted

ABSTRACT

Aims. Powerful gravitational telescopes in the form of massive galaxy clusters can be used to enhance the light collecting power over a limited field of view by about an order of magnitude in flux. This remarkable effect is exploited here to increase the depth of a survey for lensed supernovae at near-IR wavelengths.

Methods. A pilot supernova search programme conducted with the ISAAC camera at VLT is presented. Lensed galaxies behind the massive clusters A1689, A1835 and AC114 were observed for a total of 20 hours split into 2, 3 and 4 epochs respectively, separated by approximately one month to a limiting magnitude $J \lesssim 24$ (Vega). Image subtractions including another 20 hours worth of archival ISAAC/VLT data were used to search for transients with lightcurve properties consistent with redshifted supernovae, both in the new and reference data.

Results. The feasibility of finding lensed supernovae in our survey was investigated using synthetic lightcurves of supernovae and several models of the volumetric Type Ia and core-collapse supernova rates as a function of redshift. We also estimate the number of supernova discoveries expected from the inferred star formation rate in the observed galaxies. The methods consistently predict a Poisson mean value for the expected number of supernovae in the survey between $N_{\text{SN}}=0.8$ and 1.6 for all supernova types, evenly distributed between core collapse and Type Ia supernovae. One transient object was found behind A1689, 0.5'' from a galaxy with photometric redshift $z_{\text{gal}} = 0.6 \pm 0.15$. The lightcurve and colors of the transient are consistent with being a reddened Type IIP supernova at $z_{\text{SN}} = 0.62$. The lensing model predicts 1.7 magnitudes of amplification at the location of the transient, without which this object would have been hard to detected with a ground based search (unlensed magnitudes $I \sim 26.5, J \sim 25.3$).

We perform a feasibility study for the discovery potential of lensed supernovae with larger and deeper surveys and conclude that the use of gravitational telescopes is a very exciting path for new discoveries. For example, a monthly survey of a single very massive cluster with the HAWK-I camera at VLT would yield $\gtrsim 10$ lensed supernovae per year, where Type Ia supernovae would make up almost half of the expected sample.

Key words. cosmology: gravitational lensing supernovae: general

1. Introduction

Massive galaxy clusters acting as powerful gravitational telescopes offer unique opportunities to observe extremely distant galaxies (Kneib et al., 2004), as well as distant supernovae (SNe), too faint to be detected otherwise (Gunnarsson & Goobar, 2003). Lensing magnification of up to a factor ~ 40 have been inferred for many multiple images of galaxies (Seitz et al., 1998), and typical magnification factors of 5 to 10 are common within the central few arc-minutes radius of the most massive clusters of galaxies. Exploiting

this remarkable flux boost is an interesting avenue for probing the rate of exploding stars at redshifts beyond the detection capabilities of currently available telescopes. Furthermore, due to the strong lensing effect, multiple images of high- z SNe with time separations of weeks up to a few years could be observed. Such rare events could provide strong constraints on the Hubble constant, through the time delay technique (Refsdal, 1964) and possibly be used as tests of dark energy in an unexplored redshift range (Goobar et al., 2002). A feasibility study of the potential for improving the mass models of clusters of galaxies using lensed SNe will be presented in Riehm *et al.*, in preparation (Paper III).

In this paper we describe a pilot program using the ISAAC near-IR imaging camera at ESO's Very Large Telescope (VLT), aiming at detecting gravitationally lensed SNe behind very mas-

Send offprint requests to: ariel@physto.se

* Based on observations made with ESO telescopes at the La Silla Paranal Observatory under programme ID 079.A-0192 and ID 081.A-0734

sive clusters of galaxies. The potential of the scaled-up version of this project with the new HAWK-I near-IR instrument at VLT is also studied. A description of the observing strategy, the dataset and data reduction, as well as a full presentation of the photometry of the transient object discussed in Sect. 6.2, are presented in an accompanying paper (Stanishev *et al.*, in preparation, Paper I).

Throughout this paper we have adopted the concordance model cosmology, $\Omega_M = 0.3$, $\Omega_\Lambda = 0.7$, $h = 0.7$. Magnitudes are given in the Vega system.

2. Supernova subtypes

SN explosions are broadly divided into two classes, core-collapse supernovae (SN CC), marking the end of very massive stars ($\gtrsim 8M_\odot$) and the so called Type Ia supernovae (SNIa), accreting white dwarfs in close binaries where thermonuclear explosions are triggered as the system reaches the Chandrasekhar mass, $1.38M_\odot$.

Several subtypes of explosions belong to the core collapse class, including Type II SN as well as Type Ib/c and hypernovae (HN), which are also interesting because of their association with GRBs. Type II SNe are furthermore subdivided into IIP, IIL and IIn based on lightcurve and spectroscopic properties. For a recent review on SN classification and general properties, see Leibundgut (2008).

In Table 1, some of the main properties for the SNe being considered in this analysis are summarized; the peak V -band brightness, M_V , the one standard deviation around the peak intrinsic luminosity, σ_{M_V} , and the fraction of the core collapse SN subtypes, f_{CC} , as deduced from measurements of the local universe. We have adopted values of f_{CC} , lightcurve and spectral properties compiled by Peter Nugent¹, which in turn are based on work by Richardson *et al.* (2002). We note, however, that the uncertainty in the relative fractions within the core-collapse types is quite large. For instance, Smartt *et al.* (2008) found a much larger fraction of Type Ib/c (29%) than Richardson *et al.* (2002), while their estimate of the number of type IIL is about a factor 10 smaller than what has been assumed here. Clearly, significantly larger data-sets are needed to pin down the CC rates accurately, both at low and high redshifts.

Since the peak brightness, lightcurve shape and spectral energy density vary significantly between SN types, we treat each subtype separately when computing the expected rates. Synthetic lightcurves of SNe at a luminosity distance $d_L(z)$ are calculated for the observer NIR filters using cross-filter K-corrections (Kim *et al.*, 1996),

$$m_Y(z, t) = M_V(t) + \mathcal{D}(z) + K_{VY}(z, t) + \Delta m(z), \quad (1)$$

where Y stands for an arbitrary observer filter and the distance modulus is defined as:

$$\mathcal{D}(z) = 25 + 5 \log_{10} \left(\frac{d_L(z)}{1 \text{ Mpc}} \right). \quad (2)$$

The luminosity distance, d_L , in a flat ($\Omega_K = 0$) Friedmann-Lemaître-Robertson-Walker model of the universe is given by:

$$d_L(z) = c(1+z) \int_0^z \frac{dz'}{H(z')}, \quad (3)$$

¹ <http://supernova.lbl.gov/~nugent>

Table 1. Peak V -band magnitudes and their standard deviation for core collapse and Type Ia supernovae. Also shown are the differential fraction of core collapse supernovae, f_{CC} , as observed in the nearby universe (P. Nugent, private communication). A Gaussian distribution has been assumed for all types, except for Type IIL supernovae, for which a bi-Gaussian distribution is used, with the two peak values labeled IIL and IIL_{bright}.

SN type	M_V (mag)	σ_{M_V} (mag)	f_{CC}
Ia	-19.23	0.30	
IIP	-16.90	1.12	0.50
IIL	-17.46	0.38	0.2025
IIL _{bright}	-19.17	0.51	0.0675
IIn	-19.05	0.50	0.05
Ib/c	-17.51	0.74	0.15
HN	-19.20	0.30	0.03

where c denotes the speed of light in vacuum and the Hubble parameter evolves with redshift as

$$H(z) = 100 \cdot h \sqrt{\Omega_M(1+z)^3 + \Omega_\Lambda}, \quad (4)$$

in units of $\text{km s}^{-1} \text{Mpc}^{-1}$.

Also included in Eq. 1 is the perturbation $\Delta m(z) = \Delta m_{\text{ext}}(z) + \Delta m_{\text{lens}}(z)$ in the observed magnitude from lensing magnification, Δm_{lens} , and/or extinction by dust along the line of sight, Δm_{ext} .

Figure 1 shows examples of synthetic lightcurves for a representative set of SN types at redshifts $z = 1.5$ and $z = 2.0$ through the ISAAC SZ -filter ($\lambda_{\text{eff}} = 1.06 \mu\text{m}$; FWHM = $0.13 \mu\text{m}$), a broader and redder version of the more common Y filter. Due to the large lensing magnifications from the foreground cluster (Sect. 4.1), significantly higher redshifts can be probed, especially for the intrinsically fainter core collapse supernovae, but also for Type Ia supernovae beyond $z \sim 1.5$.

3. Supernova rates

In the following sections, we consider two different routes to compute the expected number of SNe in a survey. In Sect. 3.1 the volumetric approach is followed, i.e. the predictions are derived from the volume probed in the field of view of the survey and assumptions about the SN rate per co-moving volume for the various types of SNe as a function of redshift. In Sect. 3.2, we also consider the rates derived from the rest-frame UV luminosities of the resolved galaxies behind the clusters under the assumption that they trace the star formation rate in each individual galaxy.

3.1. Volumetric rate estimate

The expected number of SNe of a certain subclass, dN_j , in a redshift interval, dz , depends on the monitoring time for that specific SN type, T_j , the solid angle of the survey, ω , and the volumetric SN rate, r_V^j (with units $\text{Mpc}^{-3} \text{yr}^{-1}$):

$$dN_j = T_j(z) \cdot \frac{r_V^j(z)}{(1+z)} \cdot dV_C, \quad (5)$$

Furthermore, it is a function of cosmological parameters, since it involves the comoving volume element,

$$dV_C = \frac{cd_L^2(z)}{H(z)(1+z)^2} \omega dz. \quad (6)$$

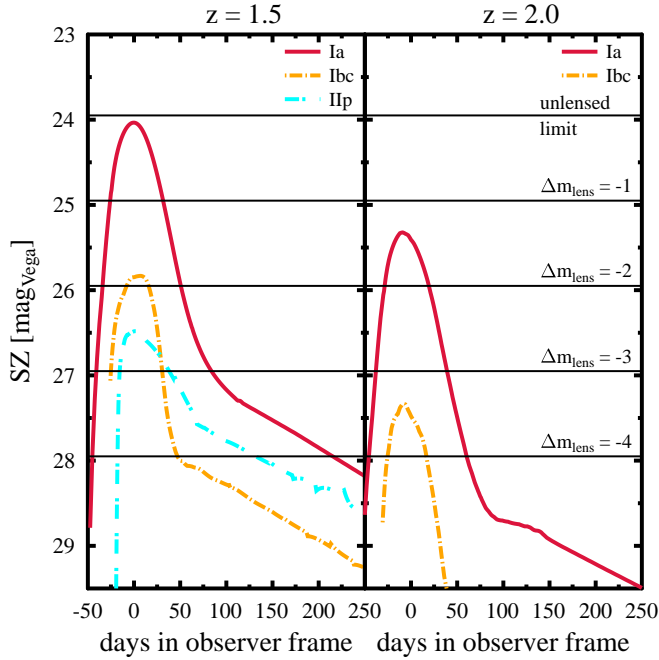


Fig. 1. Synthetic lightcurves in SZ -band of Type Ia, Type Ib/c and Type IIP supernovae at $z = 1.5$ and $z = 2$ at their mean peak brightness. Also shown is the increased sensitivity for lensing magnification by 1, 2, 3 and 4 mag. The unlensed limit, ~ 24 , corresponds to the search depth for most of the data in Table 3. Type IIP supernovae are too faint to be detected with the ISAAC survey at $z = 2$, even with $\Delta m_{\text{lens}} = -4$.

Next, we explore the current estimates of the volumetric rates of core-collapse and Type Ia supernovae.

3.1.1. Core-collapse SNe

Large scale SN programs such as SDSS, SNLS, ESSENCE or GOODS/PANS and even the planned survey at the LSST are rather inefficient at detecting core collapse SNe at $z > 1$. As an example, the two highest redshift identified CC SNe in the five year SNLS survey are at $z = 0.617$ (probable Ib/c) and $z = 0.605$ (Ib/c confirmed)². Note, however, that SNLS was specifically targeting Type Ia supernovae, and thus not optimized for finding CC SNe.

The magnification provided by foreground clusters could enable the exploration of this population for the first time. Since the progenitors of CC SNe are massive short-lived stars, the CC SN rate, r_V^{CC} , reflects the ongoing star formation rate (SFR, units $M_\odot \text{yr}^{-1} \text{Mpc}^{-3}$). Thus, we can use the SNR to obtain independent bounds on the cosmic SFR since

$$r_V^{CC}(z) = k_8^{50} \cdot \text{SFR}(z), \quad (7)$$

where $k_8^{50} = 0.007 M_\odot^{-1}$ is estimated using a Salpeter IMF (Salpeter, 1955) and a progenitor mass range between 8 and 50 solar masses, as in Dahlen et al. (2004). Although straight forward in principle, large uncertainties plague the procedure outlined in Eq. (7). The estimates of $\text{SFR}(z)$ from various data sets show a large span (Chary & Elbaz, 2001; Giavalisco et al., 2004; Hopkins & Beacom, 2006; Mannucci et al., 2007), thus leading to a very uncertain range of predictions for the SN rates, as

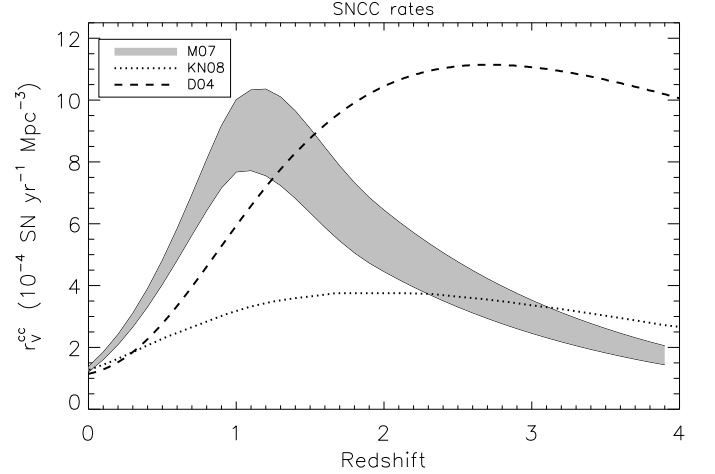


Fig. 2. Predictions for the CC SN rate, $r_V^{CC}(z)$ derived from various estimates of the star formation rate, $\text{SFR}(z)$. The shaded region (M07) is an extrapolation based on the dust corrected rate in Mannucci et al. (2007). The dashed line (D04) gives the best fit to the GOODS CC discoveries, as shown in Dahlen et al. (2004). The dotted line (KN08) shows the prediction in Kobayashi & Nomoto (2008).

shown in Fig. 2, but also allowing for the possibility to constrain the $\text{SFR}(z)$ by measuring r_V^{CC} . The estimate by Mannucci et al. (2007) (M07) shown in Fig. 2 incorporates a strong efficiency cut due to dust obscuration. The underlying assumption is that star-formation correlates with dust density. Thus, as the star formation increases with redshift, the fraction of obscured SNe increases. M07 parameterize the fraction of observable CC SNe at optical wavelengths as $f = 0.95 - 0.28 \cdot z$ for $z \leq 2$. In our work, the effective CC rate in M07 is smoothly extended up to $z \sim 4$ in a manner compatible with the upper limits on the fraction of radiation escaping high-redshift galaxies, $f \sim 0.02$ for the redshift interval $3 < z < 9$ (Gnedin et al., 2008).

The current observational results on the CC rates at high- z (Dahlen et al., 2004) show an increase in the range $z \sim 0.3 - 0.7$, consistent with independent estimates of the SFR. Extending these measurements to $z \geq 1$ is clearly important to check the underlying SFR models. Also, observations at near-IR, i.e. in the rest-frame optical, should allow a direct probe of the part of the star formation that could be missed by UV surveys due to extinction by dust in the line of sight. Since the VLT/ISAAC survey had very limited sensitivity beyond $z > 2$, the smoothly extrapolated model of M07 is mainly used for our estimate of the feasibility of discovering lensed SNe in future surveys in Sect. 7.

3.1.2. Type Ia SNe

While SNIa have been extensively used for deriving cosmological parameters, it is unsatisfactory that the progenitor scenario preceding the SN explosion is still mostly unknown. Existing models predict that different scenarios, such as the single degenerate and the double degenerate models, should have different delay-time distributions $\phi(t)$, describing the time between the formation of the progenitor star and the explosion of the SN. Recent results (Sullivan et al., 2006; Pritchett et al., 2008; Totani et al., 2008) suggest that the specific SNR (SNR per mass) is significantly higher in young star forming galaxies compared to older galaxies. These results are consistent with a power

² Kathy Perrett, private communication

law function for $\phi(t)$, suggesting that short delay-times dominate the distribution, i.e., the ‘characteristic’ delay-time τ is $\ll 1$ Gyr. These findings are consistent with the results by Mannucci *et al.* (2005), who found a factor ~ 20 higher specific SNR in late type galaxies compared to old E/S0 galaxies. Using a different method, Strolger *et al.* (2004) compare the SFR(t) and the SNR, $r_V^{Ia}(t)$, derived in the GOODS fields to derive the delay-time distribution via the relation:

$$r_V^{Ia}(t) = \nu \cdot \int_0^t \text{SFR}(t') \phi(t') dt', \quad (8)$$

where ν is the number of SNe per unit formed stellar mass. Assuming that $\phi(t)$ has a Gaussian shape, they found a most preferred delay time $\tau \sim 3\text{--}4$ Gyr, significantly longer than that found when using the specific SNR described above.

We note here that the main driver for the longer delay-time found in the method used by Strolger *et al.* (2004) is the low number of Type Ia SNe found at high redshift $z > 1.4$. It is therefore particularly important to search for SNe at these redshifts where the predicted rate is most sensitive to the delay time. If τ is large ($> 3\text{--}4$ Gyr) there should be a steep decline in the SNIa rate at $z > 1.5$, while if τ is short, the SNR should follow the SFR and remain fairly constant to $z \gtrsim 3$.

Furthermore, there are also theoretical predictions, e.g., Kobayashi *et al.* (1998) claiming that the SNIa rate could be significantly suppressed (or even inhibited) at high redshifts ($z > 2$ in spirals and $z > 2.5$ in ellipticals) due to metallicity effects. More recently, Kobayashi & Nomoto (2008) have updated their analysis and find an expected increase of the SNIa rate in elliptical hosts above $z = 2.5$. These results also show that deriving the Type Ia rate at high redshift is of high interest.

In order to calculate the number of detectable Type Ia SN, we use a sample of SNIa rate model predictions and current best fits to the available data, extrapolated to very high redshifts. These models are shown in Fig. 3. As for CC SNe, we use the smoothly extrapolated M07 model as a benchmark for the feasibility studies in Sect. 7.

3.2. SN rates derived from SFR in observed galaxies

Since the rate of SNe is expected to follow the star formation rate, we also consider the numbers that can be derived for the SFR in the galaxies detected in the field of view. In Sect. 5 we describe how galaxy catalogs were generated for the resolved objects in the line of sight of massive clusters.

In this work, we use the restframe UV luminosity as a tracer of the SFR in the observed galaxies, redshifted into the optical bands. Since the UV luminosity is thought to be generated by the most short-lived stars, it should be intimately related to star formation.

Here we use L_{2800} , the flux at rest-frame $\lambda_{eff} = 2800\text{\AA}$, to estimate the SFR. First, we use the photometric (or spectroscopic) redshift (see Sect. 5) to derive which two observed filters straddle the rest-frame L_{2800} and interpolate between these using the best-fitting spectral template to derive the apparent magnitude corresponding to the restframe L_{2800} flux. The absolute L_{2800} magnitude is thereafter derived after correcting for distance modulus and K-corrections. Next, the lensing amplification is taken into account, as described in Sect. 4.1.

Finally, we use the relation between L_{2800} and SFR from (Dahlen *et al.*, 2007) to relate the flux to star formation,

$$\text{SFR}(M_{\odot}\text{yr}^{-1}) = \frac{L_{2800}(\text{erg} \cdot \text{s}^{-1}\text{Hz}^{-1})}{7.0 \cdot 10^{27}}. \quad (9)$$

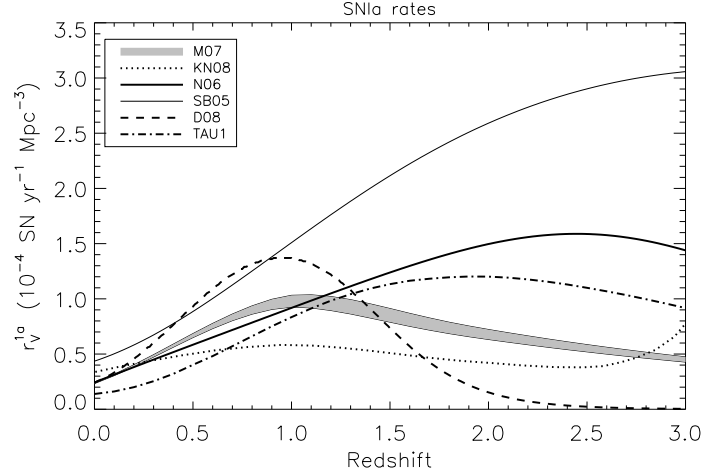


Fig. 3. Extrapolations of available SNIa rate predictions, $r_V^{Ia}(z)$. The shaded region (M07) is an extrapolation based on the dust corrected rate in Mannucci *et al.* (2007). The dashed line (D08) gives the best fit to the HST Supernova Survey (Dahlen *et al.*, 2008) corresponding to $\tau = 3.4$ Gyr. The dot-dash line (TAU1) shows the corresponding rate for $\tau = 1.0$ Gyr. In both cases a Gaussian distribution was assumed for τ . The thick solid line (N06) corresponds to the SNLS published rates in Neill *et al.* (2006). The thin solid line (SB05) stems from the so called ‘‘A+B model’’ in Scannapieco & Bildsten (2005) and the dotted line (KN08) shows the prediction in Kobayashi & Nomoto (2008).

The expected number of core collapse SNe are calculated as in Eq. (7), whereas the SNIa rate is estimated using Eq. (8) with a Gaussian distribution for $\phi(t)$ with $(\tau, \sigma) = (3.4, 0.68)$ in units of Gyr.

4. Clusters as gravitational telescopes

We have investigated the use of some of the most massive clusters of galaxies as gravitational telescopes; A1689, A1835 and AC114. A1689 ($z = 0.183$) has the largest Einstein radius of all massive lensing clusters, $\theta_E \sim 50''$. Broadhurst *et al.* (2005) and more recently Limousin *et al.* (2007) performed a strong lensing analysis using HST data and identified 115 images of 34 multiply lensed background galaxies in the redshift range $1 < z < 5.5$ based on spectroscopic and photometric redshift estimates. A cluster mass model of AC114 ($z = 0.312$, $\theta_E \sim 30''$) and several strong lenses, including a 5-image configuration at $z = 3.347$ were presented in Campusano *et al.* (2001). The mass model for A1835 ($z = 0.253$) yields an Einstein radius of $\theta_E \sim 40''$ at high- z (Richard *et al.*, 2006).

4.1. Lensing magnification: tunnel vision

To calculate the lensing magnification of the SN lightcurves, the public LENSTOOL³ software package was used. The code is specifically developed for modelling mass distribution of galaxies and clusters in the strong and weak lensing regime (Kneib *et al.*, 1996). It now uses a Monte Carlo Markov Chain technique (Jullo *et al.*, 2007) to constrain the parameters of the cluster model using observational data of the background galaxies as input. The output can then be used to compute, e.g., the

³ www.oamp.fr/cosmology/lenstool

magnification and time delay function at any given position behind the cluster. For A1689 the mass model by Limousin *et al.* (2007) was used. The clusters A1835 and AC114 have been modelled as in Richard *et al.* (2006). Figure 4 shows the average lensing magnification as a function of source redshift in the FOV of the ISAAC camera, 2.5×2.5 arc.min² for the three cluster fields considered. We note that A1689 seems to be the most promising gravitational lens for reaching the highest redshifts. For the 2007 observations of A1689 which were centered on the cluster, the amplification is on average, $\gtrsim 2.5$ mag for $z \gtrsim 1$ in the ISAAC field of view. The 2003/2004 archival observations we used were off-set from the cluster core, therefore the average amplification for these observations is smaller, ~ 1.5 mag for $z \gtrsim 1$. For A1835 the average amplification is ~ 1 mag for $z \gtrsim 1$. The width of the A1689 2003/2004 and A1835 curves indicate the slightly different pointings and effective FOV for these observations. AC114 has an average lensing amplification of ~ 0.8 mag for $z \gtrsim 1$.

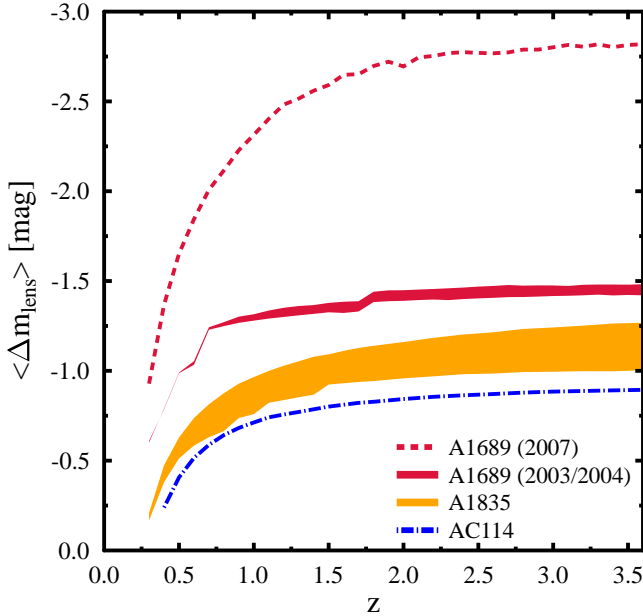


Fig. 4. Average lensing magnification vs redshift for the three observed clusters computed with LENSTOOL (see text) for the ISAAC/VLT field of view. Two curves are shown for A1689 since the pointings in 2003/2004 (dashed red) and 2007 were different. The width of the curve for the A1689 pointings (solid red) in 2003/2004 and the A1835 pointings (orange) indicate that these pointings are not covering the exact same area, but are slightly shifted between observations and the effective area observed is different (details can be found in Paper I).

4.2. Monitoring time for SN surveys with gravitational telescopes

Due to flux conservation, large lensing amplifications imply a smaller observed solid angle ω .

Therefore, unlike other SN searches, the effective solid angle ω in Eq. (6) is not constant with redshift when cluster fields are

targeted. The light beam at any given redshift behind the cluster is magnified by a factor

$$\mu = 10^{-0.4 \cdot \Delta m_{\text{lens}}}, \quad (10)$$

at the expense of a shrunk solid angle $\tilde{\omega}$ of viewing⁴

$$\delta \tilde{\omega} = \frac{\delta \omega_0}{\mu} = \delta \omega_0 \cdot 10^{0.4 \cdot \Delta m_{\text{lens}}}, \quad (11)$$

where $\delta \tilde{\omega}$ and $\delta \omega_0$ represent an infinitesimal solid angle element, with and without lensing magnification. Therefore the effective solid angle for a lensed SN search $d\tilde{V}_C$ is given by

$$d\tilde{V}_C = \frac{cd_L^2(z)}{H(z)(1+z)^2} \tilde{\omega} dz. \quad (12)$$

The corresponding shrinkage of the source area as a function of redshift for the strongest (A1689) and weakest (AC114) lens in our survey are shown in Fig. 5. The figures illustrate, that although A1689 is the most promising gravitational lens, the quick shrinkage of the solid angle with increasing redshift is also very strong⁵.

Thus, as shown in Gunnarsson & Goobar (2003), it is not always the case that looking through a gravitational lens will enhance the number of SN discoveries. On the other hand, it will always increase the limiting redshift for a magnitude limited survey. Here we exploit this effect to search for SNe at redshifts beyond what has been explored with “traditional” SN searches.

Weaker lenses such as AC114 and A1835 may not go as deep in redshift, but one may still find a comparable number of SNe as behind A1689 (or even more), although these SNe would be found at somewhat lower average redshifts.

For the unlensed case, the monitoring time above threshold for a SN of type j , T_j , is a function of the SN lightcurve, the detection efficiency, ϵ , the extinction by dust, Δm_{ext} , and the intrinsic brightness M_j with the probability distribution $P(M_j)$,

$$T_j(z, \Delta m_{\text{ext}}) = \epsilon \cdot \int \Delta t_j(z, M_j + \Delta m_{\text{ext}}) P(M_j) dM_j. \quad (13)$$

Throughout this paper we assume $P(M)$ to be Gaussian, with mean values and standard deviations listed in Table 1.

Taking into account the lensing effect of the clusters, the monitoring time becomes

$$T_j(z, \Delta m_{\text{ext}}, \Delta m_{\text{lens}}) = \epsilon \cdot \int \Delta t_j(z, M_j + \Delta m_{\text{ext}} + \Delta m_{\text{lens}}) P(M_j) dM_j, \quad (14)$$

keeping in mind that $\Delta m_{\text{ext}} > 0$ corresponds to dimmed SNe. Usually, $\Delta m_{\text{lens}} < 0$, and SNe will be magnified (although there are also a few small areas where the gravitational lens demagnifies).

Thus, the expected number of SNe for a given type j using volumetric rates is then given by

$$N_j = \int T_j(z, \Delta m_{\text{ext}}, \Delta m_{\text{lens}}) \cdot \frac{r_V^j(z)}{(1+z)} \cdot d\tilde{V}_C, \quad (15)$$

where we assume an overall Milky-Way like dust extinction (Cardelli *et al.*, 1989) with $E(B - V) = 0.15$ and $R_V = 3.1$. This choice matches the assumptions used to derive the estimates of the SFR we have used.

We obtain a map of Δm_{lens} as described in the previous section as a function of redshift, right ascension and declination.

⁴ throughout this paper $\Delta m_{\text{lens}} < 0$ for $\mu > 1$.

⁵ Gravity gives, gravity takes!

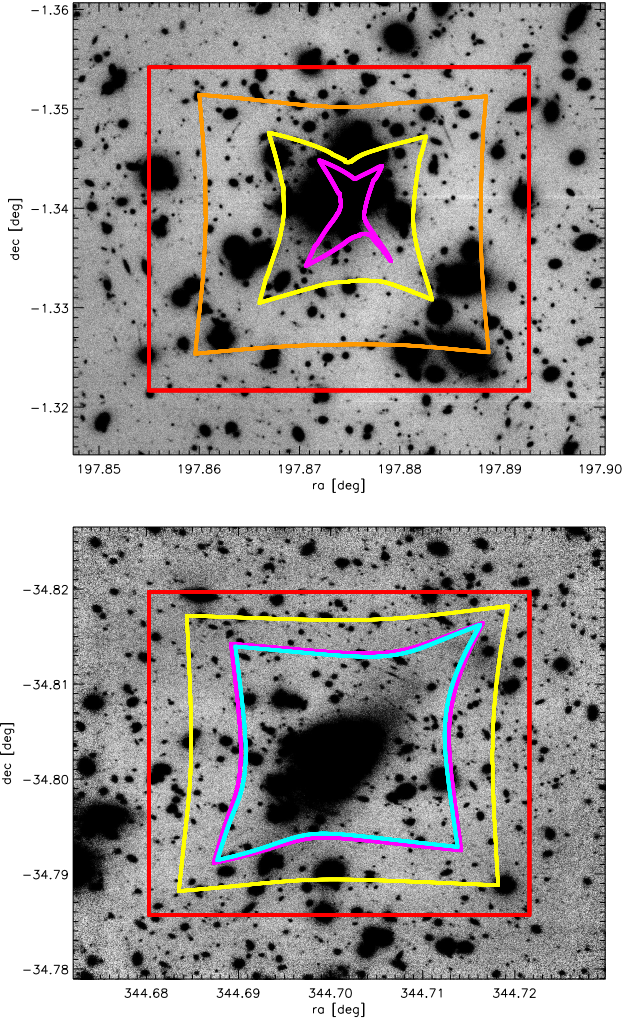


Fig. 5. Source plane area shrinkage behind our strongest gravitational telescope A1689 (top figure) for various redshifts; $z = 0.25$ (orange), 0.5 (yellow), 2.0 (magenta) and the weakest in the current survey AC114 (bottom figure) for various redshifts ($z = 0.5$ (yellow), 2.0 (magenta), 3.0 (cyan)). The utmost line (red) shows the effective FOV of the observations.

5. Properties of background galaxies

For each one of the three considered clusters, galaxy catalogs were compiled using archival optical and near-IR photometry. The different instruments and filters are listed in Table 2.

The observed magnitudes in at least three bands, optical or near-IR, were used to derive a photometric redshift using the template fitting technique, e.g. Gwyn (1995); Mobasher *et al.* (1996). Figure 6 shows the distribution of galaxies in bins of $\Delta z = 0.5$ for the three clusters. Furthermore, the restframe UV-flux at 2800\AA of each resolved galaxy was computed and used as a tracer of the SFR. Similarly, the integrated SFR was calculated in each redshift bin by summing the resolved galaxies behind each cluster. Thus, we compute the expected number of SNe from two methods; 1) the volumetric rate taken from the literature and 2) the measured star formation rate in the resolved galaxies in the FOV.

Table 2. Archival data used to calculate the photometric redshifts of the galaxies in the fields of A1689, A1835, and AC114.

Filter	Instrument/Camera
Abell 1689	
F475W, F625W, F775W, F850LP	HST/ACS
F110W, F160W	HST/NICMOS
Abell 1835	
V, R, I,	CFHT/CFH12K
F702W	HST/WFPC2
Z	VLT/FORS2
SZ, J, H, Ks	VLT/ISAAC
AC114	
U	CTIO
B	AAT/CCD1
V	ESO-NTT
F702W, F814W	HST/WFPC2
J, H, Ks	VLT/ISAAC

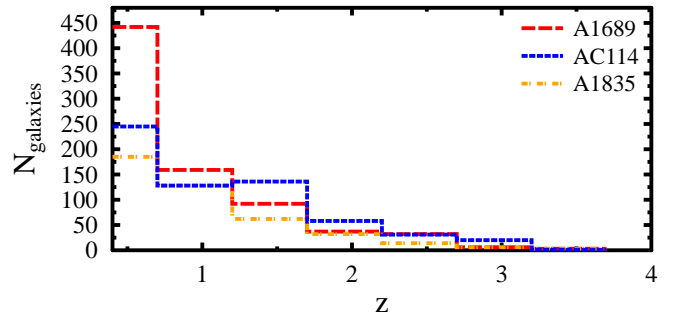


Fig. 6. Resolved galaxies vs redshift behind A1689, A1835 and AC114.

6. The ISAAC pilot survey

During the spring of 2007, three clusters, A1689, AC114 and A1835, were monitored with the ISAAC instrument at VLT with approximately one month intervals, as shown in Table 3. In total, the data set consists of 20 hours of VLT time on target: 4.5 hs, 5.85 hs and 10 hs for A1689, AC114 and A1835 respectively. The data is nicely complemented by archival data (also listed in the table): 8.4 hs, 5.7 hs and 6.1 hs for A1689, AC114 and A1835. The survey filters in our 2007 program were chosen to match the deepest reference images. Thus the SN search was done in *SZ*-filter for A1689 and A1835 and in *J*-band for AC114. A full description of the data reduction, SN search efficiency and limiting magnitude is reported in Paper I. An average discovery depth at 90 % CL of $SZ, J \lesssim 24$ mag (Vega) was derived by Monte-Carlo simulations where artificial stars were added to the images.

6.1. Expected event rate in the survey

One of the most important aspects of the pilot survey is to explore whether the use of gravitational telescopes enhances significantly the survey depth given the observational magnitude limit. In the upper panels of Figs. 7, 8, and 9 we explore the differential number of SNe expected for each one of the three clusters with lensing magnification. The lower panels of the figures show the gain/loss due to the lensing compared to the same

Table 3. Summary of archival and data allocated for this project at VLT/ISAAC on A1689, A1835 and AC114. The area in the last column corresponds to the overlap region with other images to which the detection limit in column 5 applies.

Date	Exposure [min]	Seeing [arcsec]	90% detection efficiency [mag]	Area [arcmin ²]
Abell 1689 – VLT/ISAAC <i>S</i> Z-band				
2003 02 09 ^b	159	0.52	24.28, transient	3.70
2003 04 27	43	0.43	transient	
2004 01 13	43	0.52	23.58, non-detect	
2004 02 14	43	0.58	23.64, non-detect	
2003 01 16	43	0.58	23.48	3.72
2003 02 15	43	0.50	23.60	
2003 04 27	86	0.44		
2004 01 12	43	0.55	23.64	
2007 04 08	117	0.64	23.95	4.44
2007 05 14/15	117	0.65	23.95	
2007 06 06	39	0.70	23.15	
AC 114 – VLT/ISAAC <i>J</i> -band				
2002 08 20	108	0.49	23.87	5.06
2007 07 13 ^a	234	0.43	24.04	
2007 08 09	117	0.73	23.79	
2007 09 02	117	0.55	23.83	
2007 09 28	117	0.46	24.04	
Abell 1835 – VLT/ISAAC <i>S</i> Z-band				
area 1				
2004 04 20	231	0.49	24.06	3.75
2004 05 15	135	0.62	24.06	3.75
2007 04 18	117	0.79	23.80	2.50
2007 05 18	78	0.74	23.83	3.75
2007 07 18	117	0.62	23.80	2.50
area 2				
2007 04 18	117	0.79	23.70	1.57
2007 05 14/18	60	0.80	23.45	2.13
2007 07 18	117	0.62	23.70	1.57

^a – average of observations obtained on July 11,12,13 and 15.

^b – average of observations obtained on February 5,11 and 15.

survey without lensing as a function of redshift. In particular, the lower panels indicate the redshift regions where the use of gravitational telescopes enhances the detection probability.

As expected, the boost is most important for the fainter core collapse supernovae, Type Ib/c and IIP in particular, where the detection efficiency is increased for $z > 0.5$. For the brighter SNe, like Type Ia, it is only for $z > 1$ where a net gain is to be expected. Thus, the foreground massive cluster, besides amplifying the flux, serves as a high- z filter.

AC114 and A1835 (to a somewhat lesser extent) yield comparable total SN rates as A1689 although A1689 is a much stronger lens than the other two clusters. This is due to the fact that, as already mentioned, the magnification comes along with a shrinkage of the effective volume element.

For simplicity, we restricted this comparison to the volumetric rates estimates in Mannucci et al. (2007). In Fig. 10 the various model predictions for the three clusters combined are shown for each SN type separately.

The expected total number of SNe in our survey is shown in Fig. 11. The estimated rates assume extinction by Galactic like dust (Cardelli et al., 1989) with an average color excess of $E(B - V) = 0.15$ and a total to selective extinction coefficient $R_V = 3.1$, i.e. $A_V = 0.46$ mag. Since the lensing magnification is typically $\Delta m_{\text{lens}} \lesssim -0.8$, the impact from dust extinction accounts for less than a factor two decrease in the expected number of

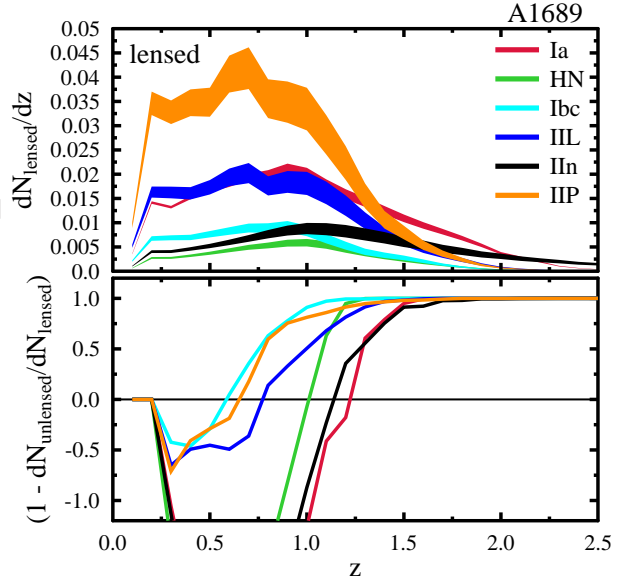


Fig. 7. Upper: Redshift distribution for the number of SNe (for each type) assuming the rates estimates by Mannucci et al. (2007) for A1689 in *SZ*-band. Lower: Gain/loss of using A1689 as a lens compared to an equivalent survey without the lens for different redshifts. The crossing of the curves through the zero line indicates the redshift for which a transition to a net gain in SN discoveries is obtained due to the gravitational telescope. An average Milky-Way like extinction with $E(B-V)=0.15$ was assumed for both plots.

SN discoveries, as compared with the results where dimming by dust is completely neglected.

6.2. A transient candidate

Image subtractions as described in Paper I were used to search for transient objects in our data set. Transients were sought for both in the new images, using the archival data as reference, and in the reverse order; searching for transients in the archival images where the period 79 data was used as a reference. The images were geometrically aligned and the point-spread functions and the flux levels of the two images were matched prior to the pixel subtraction.

In this process, one transient candidate was found in the A1689 archival images in the *SZ*-band. Luckily, also one *I*-band data point of A1689 and two *z*-band data points were observed with FORS2 and another in *J*-band with ISAAC at VLT during the time the transient was bright. We used HAWK-I *J*-band images from our program in period 81 as a reference to obtain a measurement of the transient flux in that band. Additional reference data from FORS2 and HST/ACS were available for the optical bands. These were used to measure the flux in the region of the transient after it had faded. The transient photometry is summarized in Table 4. The location of the transient and the lensing magnification map is shown in Fig. 12.

All available SN templates and a grid of redshifts ($z = [0, 3]$) and reddening parameters were tested (allowing for an intrinsic variation of the brightness) and the best fit was found for a Type IIP template based on lightcurves of SN2004et from Sahu et al. (2006), redshifted to $z_{\text{SN}} = 0.62 \pm 0.034$. Moreover, the best fit for the transient colors was found assuming the SN is highly reddened, with a low total to selective extinc-

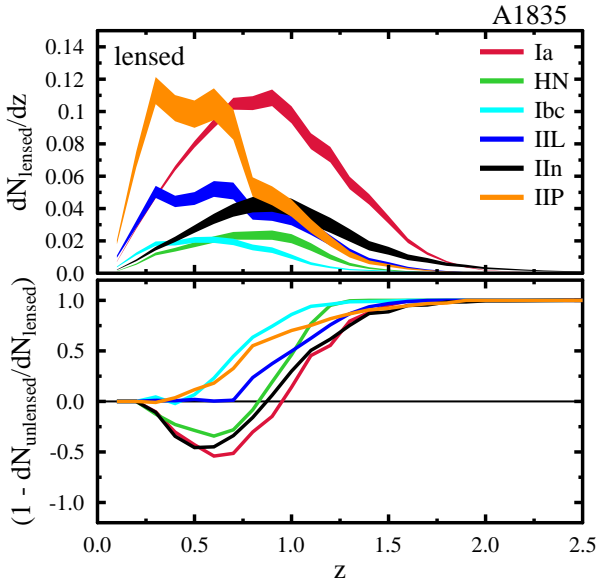


Fig. 8. Upper: Redshift distribution for the number of SNe (for each type) assuming the rates estimates by Mannucci et al. (2007) for A1835 in *SZ*-band. Lower: Gain/loss of using A1835 as a lens compared to an equivalent survey without the lens for different redshifts. The crossing of the curves through the zero line indicates the redshift for which a transition to a net gain in SN discoveries is obtained due to the gravitational telescope. An average Milky-Way like extinction with $E(B-V)=0.15$ was assumed.

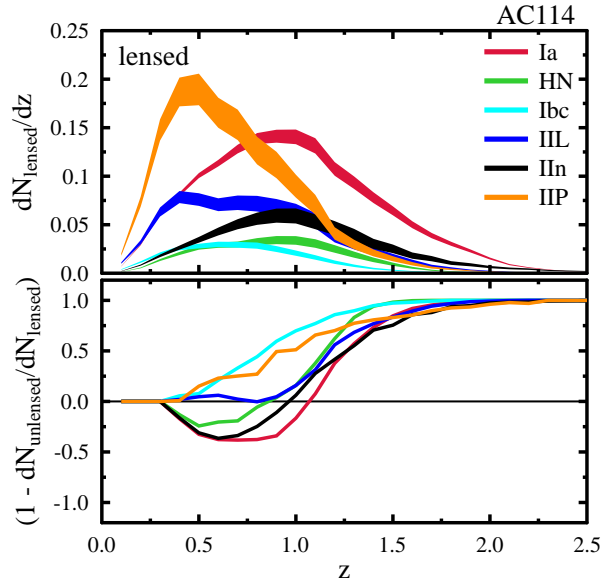


Fig. 9. Upper: Redshift distribution for the number of SNe (for each type) assuming the rates estimates by Mannucci et al. (2007) for AC114 in *J*-band. Lower: Gain/loss of using AC114 as a lens compared to an equivalent survey without the lens for different redshifts. The crossing of the curves through the zero line indicates the redshift for which a transition to a net gain in SN discoveries is obtained due to the gravitational telescope. An average Milky-Way like extinction with $E(B-V)=0.15$ was assumed.

Table 4. Transient candidate photometry from Paper I.

Date	Filter	Magnitude (mag)
2003-02-06	<i>I</i>	24.77 ± 0.20
2003-02-09/10	<i>z</i>	24.32 ± 0.07
2003-02-26/27	<i>z</i>	24.32 ± 0.08
2003-02-09	<i>SZ</i>	23.24 ± 0.08
2003-04-12	<i>J</i>	23.57 ± 0.24
2003-04-27	<i>SZ</i>	23.73 ± 0.16

tion ratio ($A_V=1.43$, $R_V=1.1$), as shown in Fig. 13. We note that low values of R_V , although not seen in the Milky Way, have been reported for extinction of quasars (Wang et al., 2004; Östman et al., 2008) and shown to be very common in SN lines of sight (Nobili & Goobar, 2008), possibly as a result of multiple scattering on circumstellar dust (Goobar, 2008). Another possibility is that the intrinsic colors of the SN candidate differ significantly from SN2004et, in which case a bias could be introduced in the K-corrections.

For the nearest galaxy, at $0.5''$ projected distance, a photometric redshift $z_{\text{gal}} = 0.60 \pm 0.15$ is derived, as shown in Fig. 14.

It should be noted, that at $z_{\text{SN}} = 0.62$, the transient ($J \sim 25.3$ mag, unlensed) would not have been detected in our survey without the amplification power of the cluster, 1.7 mag. Taking into account the lensing magnification and the assumed host galaxy extinction we find that the best fit shown in Fig. 13 corresponds to an absolute magnitude $M_V = -17.6$, in good agreement with the assumptions in Table 1.

It is striking that the tentative identification of the transient matches very well the expectations for the survey in terms of SN subtype and redshift, as shown in Fig. 7.

7. Implications for large FOV surveys

The pilot survey was obtained with the ISAAC instrument at VLT, which has a FOV of $2.5' \times 2.5'$ and a threshold of ~ 24 mag (Vega) for *SZ* and *J*-bands and relatively few observations. In this section we briefly discuss the feasibility of discoveries of lensed SNe behind clusters of galaxies for surveys with available instruments in 8-meter class ground based telescopes with large FOV near-IR instruments, such as HAWK-I at VLT or MOIRCS at Subaru. We consider a five year survey, with imaging spaced by 30 days.

The lensing model of A1689 is used as our baseline for estimating the number of SNe behind a massive cluster as a function of redshift. Thus, the results below apply for the most massive clusters, $M \sim 10^{15} M_{\odot}$. We also consider a survey period of five years since this is optimal for the discovery of multiple images (Sect. 7.1). In practice, several clusters would have to be observed to match the correspondence to '5 A1689 years' since that field is behind the sun parts of the year.

During period 81 (P81), our team started a survey targeting lensed SNe behind A1689 using the large HAWK-I camera FOV ($\approx 7.5' \times 7.5'$) on VLT. Due to the limited availability of the instrument in P81, only a few, closely spaced observations were done. Although the observations were not suitable for transient searches, the data-set could be used to estimate the depth of the point source search in *J*-band to be continued during P82 to ~ 24.65 mag (Vega) for 90% detection efficiency.

In the upper panel of Fig. 15, the differential number of SNe is shown for the various types of SNe. The lower part of the figure shows the gain/loss due to the lensing compared to the same survey without lensing as a function of redshift. As expected, fewer SNe are found at low redshifts while the survey depth is

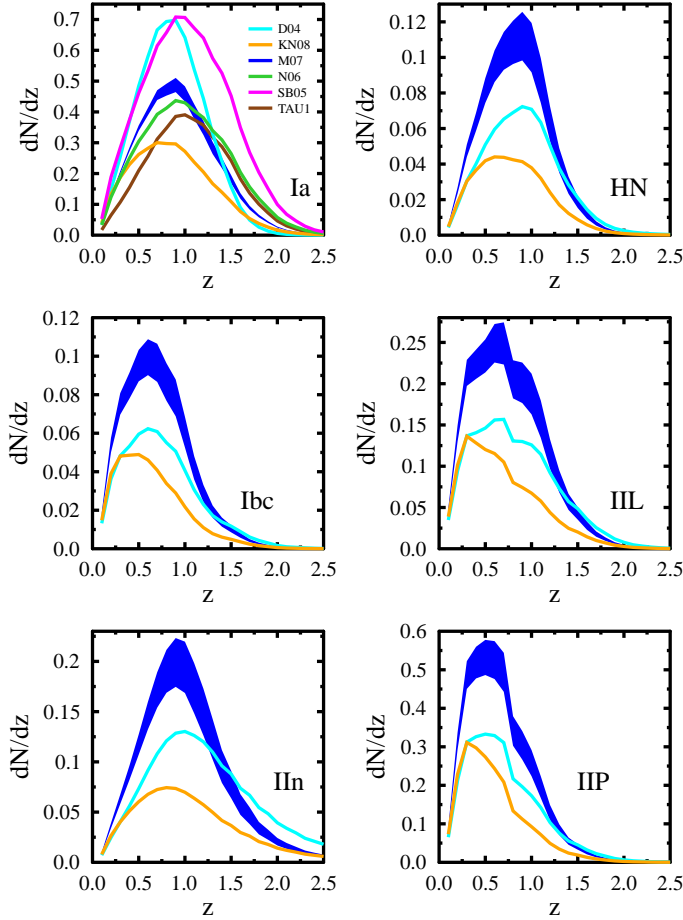


Fig. 10. Redshift distribution (including an overall reddening of $E(B - V) = 0.15$ and $R_V = 3.1$) for the number of SNe for the various model predictions for the three clusters combined for each SN type separately.

significantly increased. The integrated number of SNe for the various models is shown in Fig. 16.

For HAWK-I (and the A1689 mass model), we expect on the order of 40-70 SNe (depending on the underlying rate estimate for the various SN types) of which about a dozen will be at $z > 1.5$. Surveys for lensed supernovae with space instruments would be complementary to the ground based approach since even higher redshifts could be reached thanks to the deeper point source sensitivity.

7.1. Multiple SN images

When looking through gravitational lenses, multiple images of the same source image can be observed. This is also true for SNe that, due to strong lensing, could potentially be detected to very high redshifts. About one in a hundred SNe behind A1689 in the HAWK-I FOV would have multiple images with time separations between weeks and a few years. Thus, about 0.5-1.0 SNe with multiple images are expected in a 5 year survey with HAWK-I.

Figure 17 shows what fraction of the source areas with multiple lensed SNe can be observed as a function of survey time for two different redshifts. For $z = 1$, all SN types show the same behavior and given a sufficiently large survey time, at least two

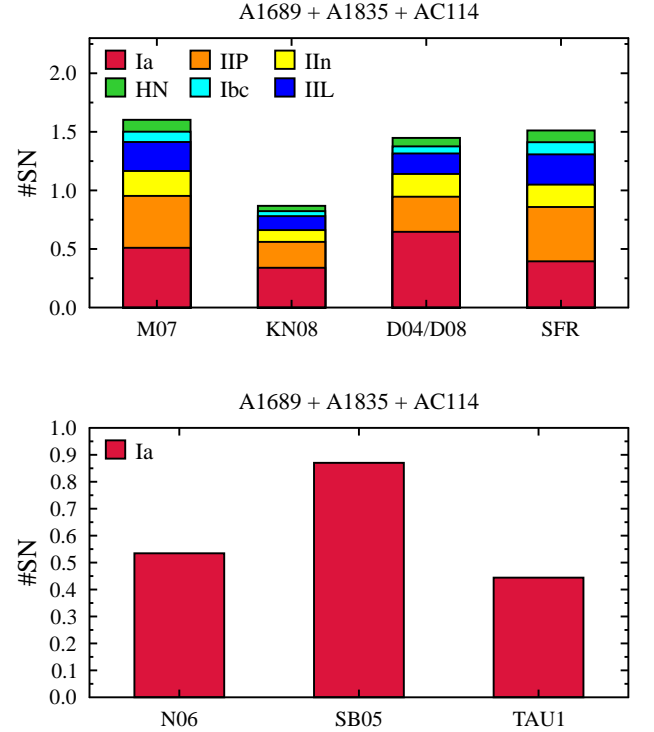


Fig. 11. Number of expected SNe for the observations given in Table 3 for (1) the SN rates shown in Figs. 2 and 3, and (2) the SN rates derived from SFR (denoted by SFR) in resolved galaxies described in Sect. 3.2.

(or more) images of the SN could be observed, regardless of its type. At higher redshifts ($z = 2$), given a sufficiently large survey time, most of the brighter SNe (Ia and IIn) and about half of the IIL_{bright} and HN will be observable and at least have two (or more) images. The other SN types (IIL, Ibc, and IIP) will be too faint – even with magnification – to be observed. For all considered redshifts, a 5 year survey (or longer) is optimal for discovering multiple images of SNe behind clusters.

Detecting such rare events could provide strong constraints on the Hubble constant through the time delay technique (Refsdal, 1964) as well as having the potential to test dark matter and energy properties in an unexplored redshift range (Goobar *et al.*, 2002; Mörtzell & Sunesson, 2006).

8. Conclusions

Powerful gravitational telescopes in the form of massive galaxy clusters present a unique opportunity to discover transient objects like SNe at redshifts beyond what can be reached with current telescopes. Thanks to the recent deployment of large FOV near-IR cameras, such as HAWK-I at VLT, the search for the highest redshift SNe can now be moved to longer wavelengths, thus avoiding the difficulties involved with doing restframe UV observations.

A combined 40 hour data-set involving archival ISAAC data and new observations obtained in 2007 for three very massive clusters (A1689, A1835 and AC114) was used as a test bed for the feasibility to discover lensed core collapse and Type Ia SNe. Considering the monitoring time available, the area surveyed, the lensing magnification and the survey magnitude limit rates estimates for the various SN subtypes considered

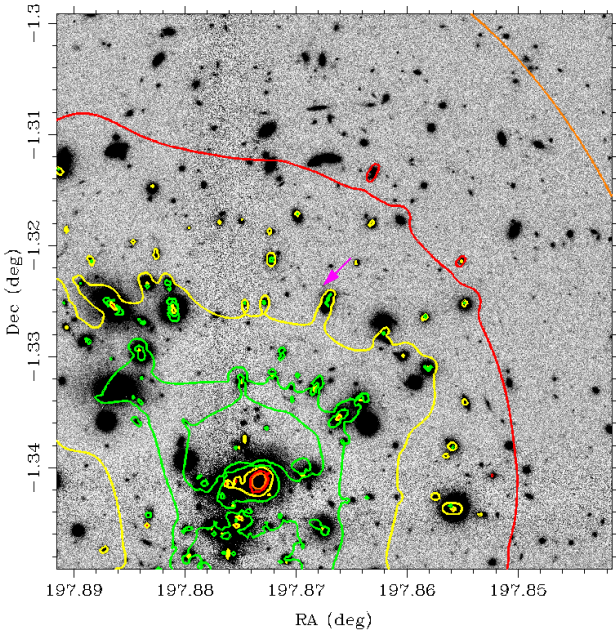


Fig. 12. LENSTOOL lensing amplification map of A1689 based on mass model in Limousin et al. (2007) superimposed on top of a HAWKI *J*-band image from our P81 program. The lensing contours for a source at $z = 0.62$ for $\Delta m_{\text{lens}} = (-0.5, -1, -2, -5)$ mag shown in (orange, red, yellow, green). The arrow points to the position of the transient, where a magnification of 1.7 mag is expected.

were calculated. Synthetic lightcurves of SNe and several models of the volumetric Type Ia and core-collapse SN rates as a function of redshift were used, all consistently predicting a Poisson mean value for the expected number of SNe in survey between $N_{\text{SN}} = 0.8$ and 1.6 for all SNe. One transient object was found behind A1689 on a galaxy with photometric redshift $z_{\text{gal}} = 0.6 \pm 0.15$, the most probable redshift for SN detection in the ISAAC/VLT survey. The lightcurve is consistent with being a reddened Type IIP supernova at $z_{\text{SN}} = 0.62 \pm 0.034$. At the position and redshift of the transient, the lensing model predicts 1.7 magnitudes of amplification.

A feasibility study for the discovery potential of lensed SNe with larger and deeper surveys shows that this is a very exciting path for new discoveries. E.g., the equivalent of a five year monthly survey of a single very massive cluster with the HAWK-I camera at VLT would yield 40 – 70 lensed SNe. Thus, a dedicated multi-year NIR imaging campaign targeting several massive clusters would lead to a dramatic discovery rate of very high- z SNe, otherwise unobservable with current instrumentation.

Although very rare, multiple images of strongly lensed SNe are within reach of such a survey and could potentially offer exciting tests of cosmological parameters as well as improvements of the cluster mass modelling.

Acknowledgements

We would like to thank Peter Nugent for providing lightcurve and spectral templates used in this analysis. Filippo Mannucci is also thanked for making his SN rate predictions available

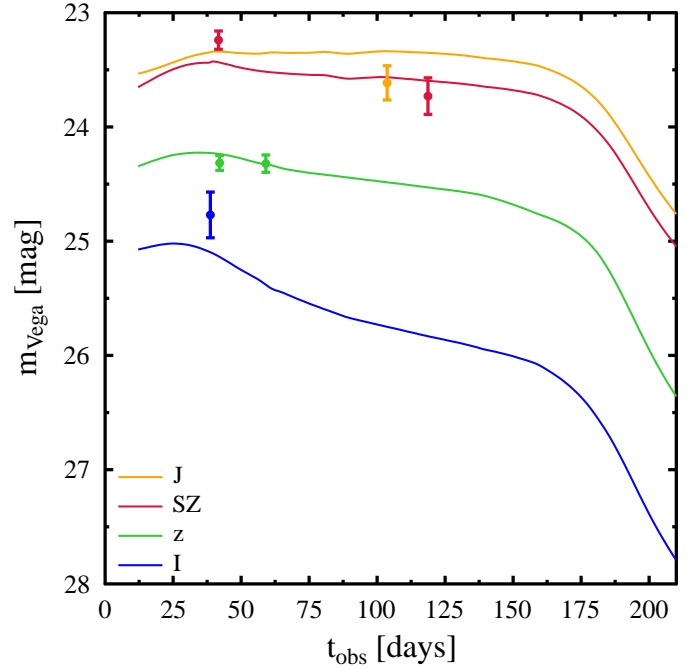


Fig. 13. Transient candidate photometry (also listed in Table 4) plotted on top of redshifted ($z_{\text{SN}} = 0.62$) lightcurves of the very well observed Type IIP SN SN2004et (Sahu et al., 2006). The nearby SN lightcurves were K-corrected using IIP spectral templates derived from spectra and photometry of SN2004et and reddened following the extinction law in Fitzpatrick (1999) with the parameters $E(B - V) = 1.3$ and $R_V = 1.1$.

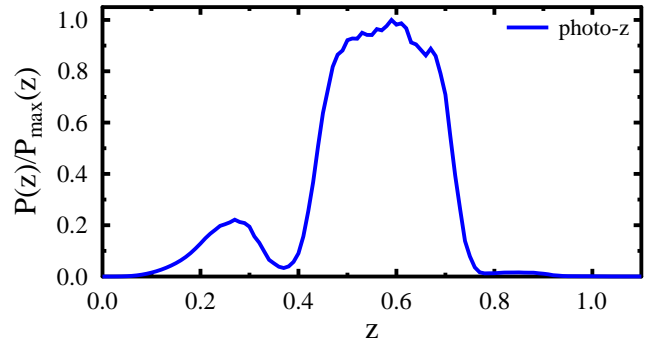


Fig. 14. Probability distribution function for the photometric redshift (seven bands) of the galaxy closest (0.5 arcseconds) to the transient.

to us. KP gratefully acknowledges support from the Wenner-Gren Foundation. AG, VS and SN acknowledge support from the Gustafsson foundation. AG and EM acknowledge financial support from the Swedish Research Council. JPK thanks CNRS for support as well as the French-Israeli council for Research, Science and Technology Cooperation.

References

- Broadhurst, T. et al. 2005, *ApJ*, 621, 53
- Campusano, L. E., Pelló, R., Kneib, J.-P., Le Borgne, J.-F., Fort, B., Ellis, R., Mellier, Y., & Smail, I. 2001, *A&A*, 378, 394
- Cardelli, J. A., Clayton, G. C., & Mathis, J. S. 1989, *ApJ*, 345, 245

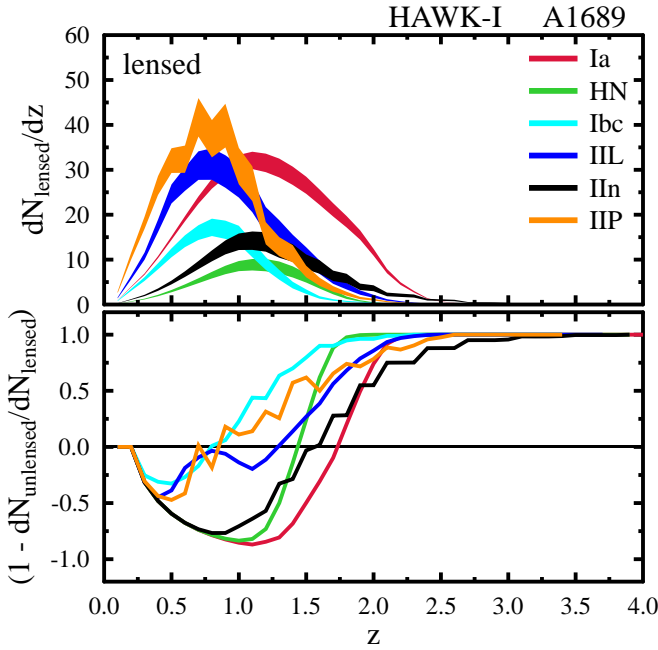


Fig. 15. Upper: Redshift distribution of SN discoveries in a 5 year survey behind a very massive cluster (model of A1689 used). Lower: Gain/loss of using a A1689 as a lens compared to an equivalent survey without the lens for different redshifts. The crossing of the curves through the zero line indicates the redshift for which a transition to a net gain in SN discoveries is obtained due to the gravitational telescope. An average Milky-Way like extinction with $E(B-V)=0.15$ was assumed together with SN rates from M07.

Chary, R., & Elbaz, D. 2001, *ApJ*, 556, 562
Dahlen, T., Mobasher, B., Dickinson, M., Ferguson, H. C., Giavalisco, M., Kretchmer, C., & Ravindranath, S. 2007, *ApJ*, 654, 172
Dahlen, T., Strolger, L.-G., & Riess, A. G. 2008, *ApJ*, 681, 462
Dahlen, T. et al. 2004, *ApJ*, 613, 189
Fitzpatrick, E. L. 1999, *PASP*, 111, 63
Giavalisco, M. et al. 2004, *ApJ*, 600, L103
Gnedin, N. Y., Kravtsov, A. V., & Chen, H.-W. 2008, *ApJ*, 672, 765
Goobar, A. 2008, *ApJ*, 686, L103
Goobar, A., Mörtzell, E., Amanullah, R., & Nugent, P. 2002, *A&A*, 393, 25
Gunnarsson, C., & Goobar, A. 2003, *A&A*, 405, 859
Gwyn, S. D. J. 1995, Master's thesis, MS Thesis, University of Victoria (1995)
Hopkins, A. M., & Beacom, J. F. 2006, *ApJ*, 651, 142
Jullo, E., Kneib, J.-P., Limousin, M., Elíasdóttir, Á., Marshall, P. J., & Verdugo, T. 2007, *New Journal of Physics*, 9, 447
Kim, A., Goobar, A., & Perlmutter, S. 1996, *PASP*, 108, 190
Kneib, J.-P., Ellis, R. S., Santos, M. R., & Richard, J. 2004, *ApJ*, 607, 697
Kneib, J.-P., Ellis, R. S., Smail, I., Couch, W. J., & Sharples, R. M. 1996, *ApJ*, 471, 643
Kobayashi, C., & Nomoto, K. 2008, *ArXiv:0801.0215*
Kobayashi, C., Tsujimoto, T., Nomoto, K., Hachisu, I., & Kato, M. 1998, *ApJ*, 503, L155+
Leibundgut, B. 2008, *General Relativity and Gravitation*, 40, 221
Limousin, M. et al. 2007, *ApJ*, 668, 643
Mannucci, F., Della Valle, M., & Panagia, N. 2007, *MNRAS*, 377, 1229
Mannucci, F., Della Valle, M., Panagia, N., Cappellaro, E., Cresci, G., Maiolino, R., Petrosian, A., & Turatto, M. 2005, *A&A*, 433, 807
Mobasher, B., Rowan-Robinson, M., Georgakakis, A., & Eaton, N. 1996, *MNRAS*, 282, L7
Mörtzell, E., & Sunesson, C. 2006, *Journal of Cosmology and Astro-Particle Physics*, 1, 12
Neill, J. D. et al. 2006, *AJ*, 132, 1126
Nobili, S., & Goobar, A. 2008, *A&A*, 487, 19
Östman, L., Goobar, A., & Mörtzell, E. 2008, *A&A*, 485, 403
Pritchett, C. J., Howell, D. A., & Sullivan, M. 2008, *ApJ*, 683, L25
Refsdal, S. 1964, *MNRAS*, 128, 307
Richard, J., Pelló, R., Schaerer, D., Le Borgne, J.-F., & Kneib, J.-P. 2006, *A&A*,

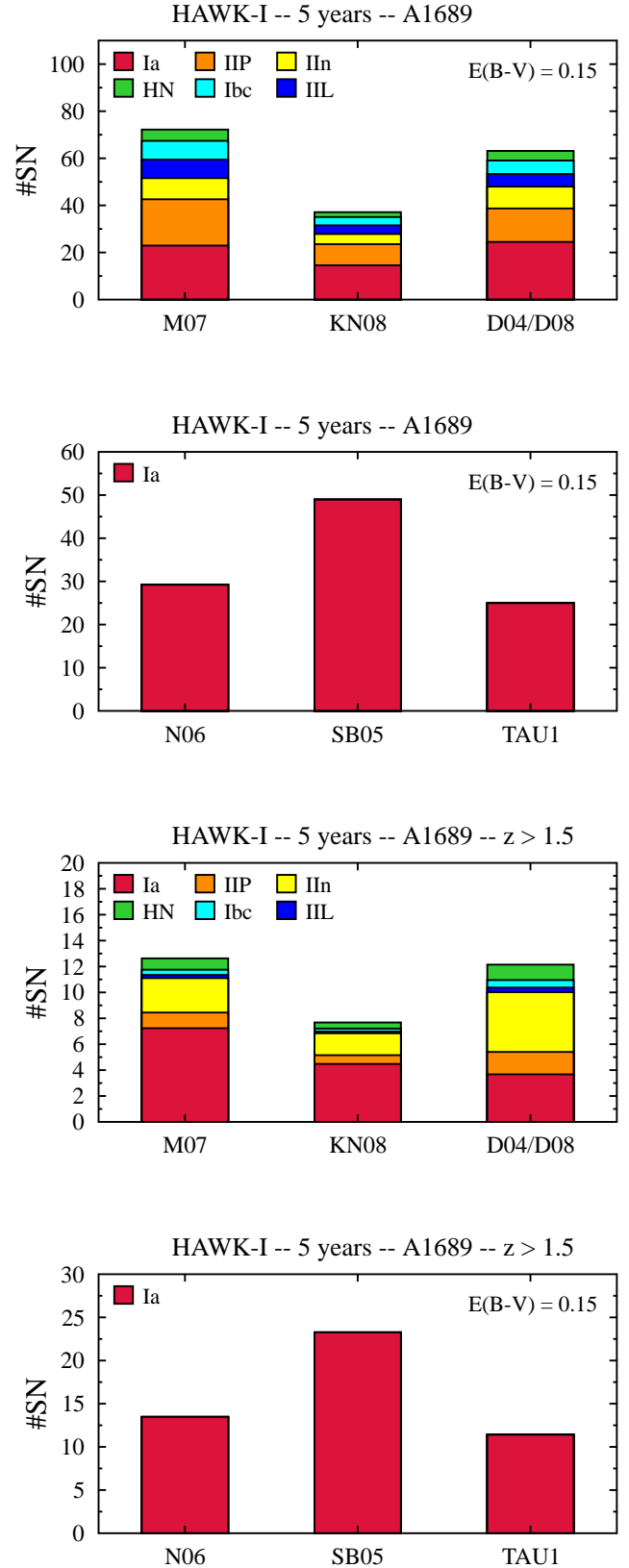


Fig. 16. (Top) Number of SNe expected in a 5 year monthly survey of one very massive, A1689-like cluster, with HAWK-I. (Bottom) Number of SNe with $z > 1.5$.

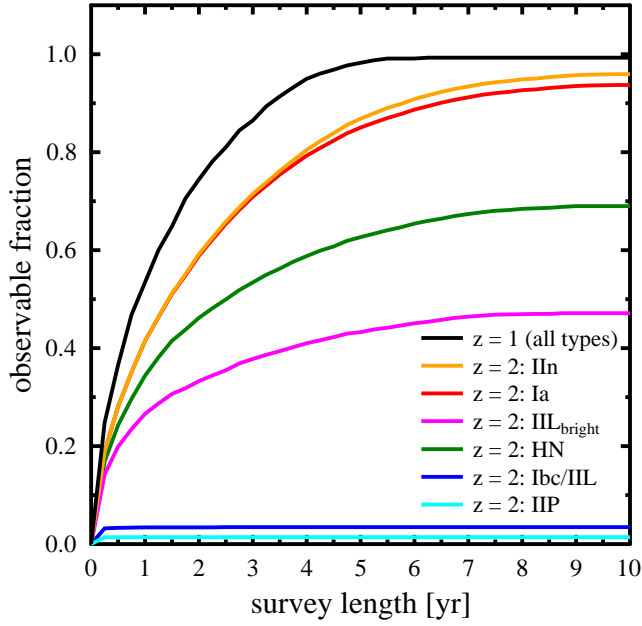


Fig. 17. Fraction of the SN with multiple images that are observable as a function survey length.

456, 861

Richardson, D., Branch, D., Casebeer, D., Millard, J., Thomas, R. C., & Baron, E. 2002, *AJ*, 123, 745

Sahu, D. K., Anupama, G. C., Sridhya, S., & Muneer, S. 2006, *MNRAS*, 372, 1315

Salpeter, E. E. 1955, *ApJ*, 121, 161

Scannapieco, E., & Bildsten, L. 2005, *ApJ*, 629, L85

Seitz, S., Saglia, R. P., Bender, R., Hopp, U., Belloni, P., & Ziegler, B. 1998, *MNRAS*, 298, 945

Smartt, S. J., Eldridge, J. J., Crockett, R. M., & Maund, J. R. 2008, *arXiv:0809.0403*

Strolger, L.-G. et al. 2004, *ApJ*, 613, 200

Sullivan, M. et al. 2006, *ApJ*, 648, 868

Totani, T., Morokuma, T., Oda, T., Doi, M., & Yasuda, N. 2008, *arXiv:0804.0909*

Wang, J., Hall, P. B., Ge, J., Li, A., & Schneider, D. P. 2004, *ApJ*, 609, 589